ISSN 1063-7850, Technical Physics Letters, 2020, Vol. 46, No. 2, pp. 118–121. © Pleiades Publishing, Ltd., 2020.
Russian Text © The Author(s), 2020, published in Pis'ma v Zhurnal Tekhnicheskoi Fiziki, 2020, Vol. 46, No. 3, pp. 19–22.

The Effect of Plastification of Cu–14Al–4Ni Alloy with the Shape Memory Effect in High-Temperature Isothermal Precipitation

A. E. Svirid[a,b], V. G. Pushin[a,b]*, N. N. Kuranova[a,b], E. S. Belosludtseva[a], A. V. Pushin[a,b], and A. V. Lukyanov[c]

[a] *M.N. Mikheev Institute of Metal Physics, Ural Branch, Russian Academy of Sciences, Yekaterinburg, 620108 Russia*
[b] *B.N. Yeltsin Ural Federal University, Yekaterinburg, 620075 Russia*
[c] *St. Petersburg State University, St. Petersburg, 199034 Russia*
**e-mail: pushin@imp.uran.ru*

Received April 2, 2019; revised October 31, 2019; accepted October 31, 2019

Abstract—It was found that deformation by the uniaxial compression scheme (while measuring mechanical properties under isothermal conditions) at 600–800°C leads to a significant refinement of the grain structure, which increases the strength and ductility of Cu–13.95 wt % Al–3.98 wt % Ni alloy, experiencing thermoelastic martensitic transformation and related shape memory effects. The structural and phase composition features were studied using scanning and transmission electron microscopy and X-ray diffraction.

Keywords: Cu–Al–Ni alloy, isothermic precipitation, thermoelastic martensitic transformations, fine-grained structure, mechanical properties.

DOI: 10.1134/S1063785020020145

Alloys based on the Ti–Ni and Cu–Al systems and a number of others represent a class of materials with shape memory effects (SMEs), which are caused by thermoelastic martensitic transformations (TMTs) [1]. It is known that special requirements of high long-term reliability during operation under cyclic changes in a fairly wide temperature range [2] are required for the service characteristics of devices made of SME alloys. However, despite the variety of developed materials with the SME, even in the case of Ti–Ni alloys with an unique complex of mechanical properties, only their binary compositions are widely used, and in a narrow doping range (from 49.5 to 50.5 at % Ni) [2]. Copper alloys of the Cu–Al, Cu–Al–Ni, and Cu–Al–Zn systems are characterized by better thermal and electrical conductivity and manufacturability, as well as lower cost, in comparison with Ti–Ni, and they have superior SME characteristics in the single-crystal state [1–6]. At the same time, the overwhelming majority of nonferrous alloys with the SME, including copper-based β alloys, in the usual polycrystalline state have extremely low ductility, cyclic strength, and durability that does not allow the implementation of their inherent SME [1, 6, 8–12], in contrast to Ti–Ni [1, 2, 7].

One of the main specific reasons for the brittleness of metastable copper β bcc alloys with respect to TMTs is a high anisotropy of elastic moduli $A = C_{44}/C'$, close to 12–13 [13], in contrast to elastically isotropic and ductile titanium nickelide alloys, for which $A = 1–2$ [14]. When highly anisotropic elastic stresses accumulate in alloys due to TMTs, they are localized primarily at grain boundaries, drastically weakening them, especially in coarse-grained (CG) alloys [1, 6]. Other causes of severe embrittlement are the high localization of impurities and precipitates of excess phases at the grain boundaries and, as a rule, coarse- and differently grained copper alloys [1, 6, 15, 16].

It is known that, due to the decrease in grain size, it is possible to significantly increase the strength and plastic properties of Ti–Ni [7] and Cu–Al–Ni [6, 9, 11, 16–18] alloys. To grind the grain structure in such alloys, attempts have been made to use various alloying additives, methods of synthesis and processing: heat treatment and forging [17, 18], thermal cycling under load [4], and ultrafast casting of the melt [11, 16]. The methods of torsion under pressure and equal-channel angular pressing have proven to be an effective way to obtain fine-grain (FG) and ultrafine grain alloys [7, 17–20]. In the present work, for Cu–Al–Ni alloy with a TMT and SME, a new method of warm controlled precipitation was used at temperatures above the eutectoid decay boundary; for the first time, we studied the features of microstructure formation,

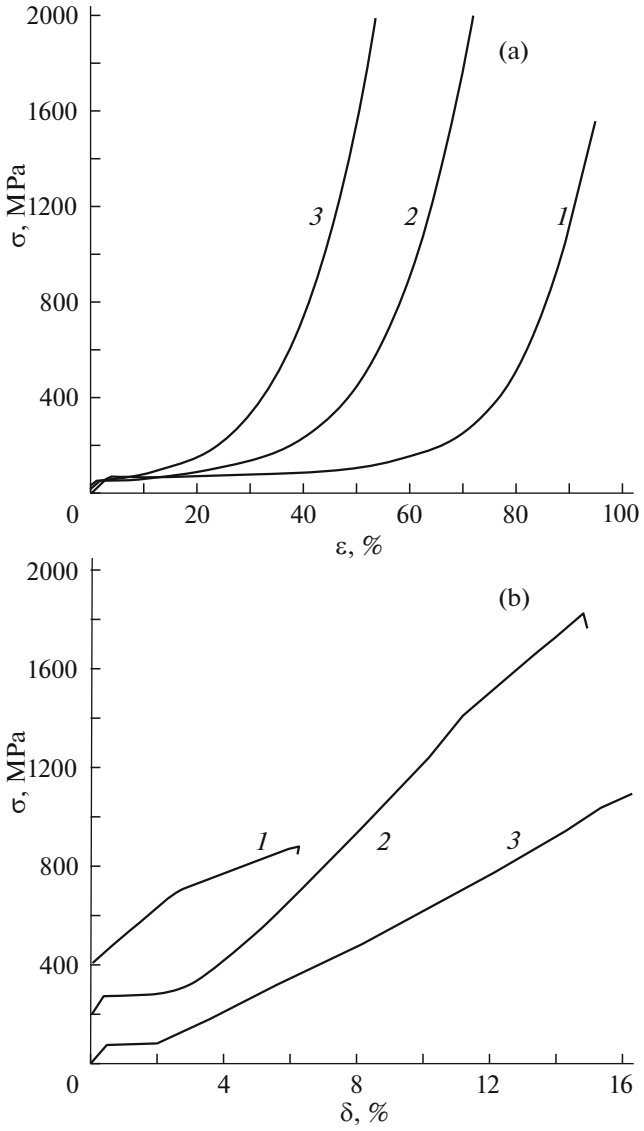

Fig. 1. Stress–strain curves of deformation of Cu–14Al–4Ni alloy obtained by compression tests at (a) (*1*) 600, (*2*) 700, and (*3*) 800°C and (b) under subsequent tension at temperatures of (*1*) 20, (*2*) 700, and (*3*) 800°C after upsetting.

mechanical properties, and destruction mechanisms of the alloy after various external effects.

One of the most studied alloys, including in the above-mentioned works [1–6, 8–13, 15–18], was selected for study—Cu–13.95 wt %–Al 3.98 wt % Ni (Cu–14Al–4Ni), obtained from Cu, Al, and Ni with a purity of 99.99%. The ingot was homogenized at 900 ± 25°C; then, at 950°C it was rolled into a bar with a cross section of 20 × 20 mm. After repeated heating at 950°C (10 min), the alloy was quenched in water at room temperature. Uniaxial compression was carried out in an Instron 8862 electromechanical measuring system equipped with an electric furnace under isothermal conditions at temperatures of 600–800°C on standard cylindrical alloy samples with a diameter d_0 = 7.5 mm and height h_0 = 9.2 mm at a test speed of 1 mm/min. The spectral chemical composition and phase composition were studied by X-ray diffraction on the initial cast CG sample (with grain sizes up to 1 mm) and the resulting FG samples resulting from precipitation. Microstructural studies were carried out using scanning electron microscopy (SEM) and transmission electron microscopy (TEM) with the equipment of the Center for Collective Use of the Institute of Metal Physics, Ural Branch, Russian Academy of Sciences, after sample preparation by fine mechanical grinding, chemical etching (for SEM), and finish electrolytic thinning (for TEM).

In the course of testing the mechanical properties in the process of isothermal compression in the austenitic state at 600, 700, and 800°C, high mechanical characteristics of the alloy were established (Fig. 1a, Table 1). Starting from low stresses of yield strength σ_y (less than 100 MPa), the alloy experienced uniform deformation ε_{st} (up to 50% at 600°C), then, at the final stage of plastic deformation up to destruction ε_f (up to 95%), it experienced strong deformation strengthening at high ultimate strength σ_u. It was found that, during compression, specific processes of continuous dynamic recrystallization take place under the impact of load, which was first minimal at the steady-state stage of uniform plastic flow and, then, increased sharply (up to 2 GPa). As a result, this led to the formation of an equal axis FG structure in the initial CG alloy, the average dimensions of which turned out to be an order of magnitude smaller than according to SEM data and amounted to 300 and 100–120 μm after precipitation testing at temperatures of 600 and 700–800°C (Figs. 2a, 2b). Upon cooling to room temperature, TMT occurred with the appearance of thin-plate martensite, usually with single-packet micromorphology within grains (Fig. 2b) in the FG alloy. The existence of a pairwise twin structure of packet martensite follows from the analysis of TEM data (Fig. 2c).

Table 1. Mechanical properties during uniaxial compression at temperatures of 600, 700, and 800°C

T, °C	σ_u, MPa	σ_y, MPA	ε_{st}, %	ε_f, %
600	1600	70	50	95
700	2000	50	20	70
800	2000	50	10	55

Table 2. Mechanical properties during tensile tests of alloy at room temperature

Treatment	σ_u, MPa	σ_m, MPa	δ_f, %	ε_m, %
Quenching at 950°C	500	300	6	–
Precipitation at 700°C	1600	80	14	3
Precipitation at 800°C	1100	80	16	2

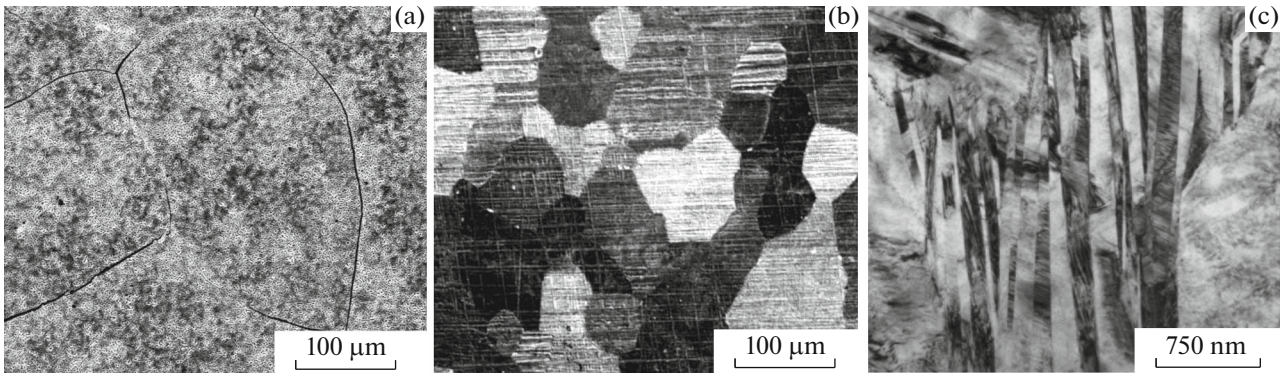

Fig. 2. (a, b) SEM and (c) TEM images of the microstructure of alloy after hot upsetting at (a) 600 and (b, c) 700°C.

The results of subsequent mechanical tests under tension of alloy in a martensitic state are presented in Fig. 1b. The characteristics of FG alloy after precipitation were measured at 700 and 800°C, and CG alloy was compared in the initial state after forging at 950°C and quenching (Table 2). A unique feature of mechanical behavior of FG alloy under tension after precipitation was the appearance of a state of martensitic nonelastic pseudofluidity, which was ε_m 2–3% at low stress of the beginning of reorientation of twin martensitic structure ($\sigma_m < 100$ MPa). When the load is further increased, deformation takes place under conditions of strong strengthening and finishing by the destruction of samples at high σ_u after significant plastic deformation for such alloys $\delta_f = 14–16\%$ (curves *2*, *3* in Fig. 1b). Curve *1* shows the low strength and plastic properties of the initial CG alloy, on the other hand.

A typical fractographic image of fractures after tensile testing of the alloy is shown in Fig. 3. Despite a rather large plastic deformation and uniform elongation (14–16%), according to the type of fracture surfaces, it can be concluded that fracture occurred simultaneously by viscous and quasi-brittle mechanisms. On the fracture surface of discontinuous samples after precipitation, cup- and ridge-shaped zones of viscous fracture and smooth chips and cracks were visible, both at the grain boundaries and at the boundaries of dispersed martensite packets (Fig. 3). However, in this case, the linear dimensions of the flat elements of the fracture surfaces were more than an order of magnitude smaller than the grain sizes, which implies that quasi-brittle fracture occurred primarily along the interfaces of dispersed martensite packets.

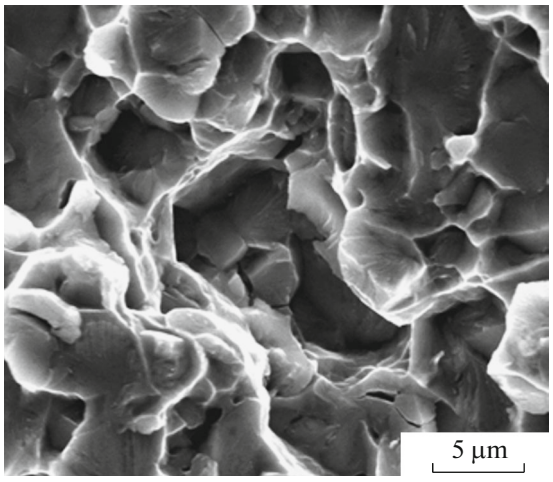

Fig. 3. Typical SEM image of a viscous–brittle fracture surface after mechanical tensile tests of alloy subjected to upsetting at a temperature of 700°C.

Thus, in uniaxial compression in a testing machine within the temperature range of 600–800°C, the plasticization effect was found of the Cu–13.95 wt % Al–3.98 wt % Ni alloy as a result of its dynamic recrystallization into the austenite FG structure, which is capable of developed plastic deformation. Subsequent cooling to room temperature, without changing the FG structure, led to the appearance of martensite of single-packet morphology with a uniform distribution of dispersed pairwise twin martensitic crystals over the alloy volume, which ensured favorable accommodation of elastic bulk and shear stresses due to the TMT. As a result, destruction of the FG alloy under uniaxial tension occurred after significant hardening and plastic deformation by viscous small-pit and viscous–brittle (along the boundaries of dispersed packets) intragranular fracture mechanisms, which resulted in its increased ductility and viscosity in the martensitic state.

FUNDING

This work was financially supported by state assignment no. AAAA-A18-118020190116-6 (“Structure“) of the Institute of Metal Physics, Ural Branch, Russian Academy of Sciences, and the joint laboratory of the Institute of Metal Physics and Ural Federal University.

CONFLICT OF INTEREST

The authors declare that they have no conflict of interest.

REFERENCES

1. K. Ootsuka, K. Simidzu, Yu. Sudzuki, Yu. Sekiguti, Ts. Tadaki, T. Khomma, and S. Miyadzaki, in *Shape Memory Effects in Alloys*, Ed. by J. Perkins (Plenum, New York, 1975; Metallurgiya, Moscow, 1990).
2. *Materials with Shape Memory Effect*, Ed. by V. A. Likhachev (NIIKh SPbGU, St. Petersburg, 1997–1998) [in Russian].
3. S. A. Pul'nev, V. I. Nikolaev, G. A. Malygin, S. L. Kuz'min, V. V. Shpeizman, and S. P. Nikanorov, Tech. Phys. **51**, 1004 (2006).
4. L. A. Matlakhova, E. C. Pereira, A. N. Matlakhov, S. N. Monteiro, and R. Toledo, Mater. Charact. **59**, 1630 (2008).
5. V. I. Nikolaev, P. N. Yakushev, G. A. Malygin, A. I. Averkin, A. V. Chikiryaka, and S. A. Pulnev, Tech. Phys. Lett. **40**, 123 (2014).
6. R. Dasgupta, J. Mater. Res. **29**, 1681 (2014).
7. V. G. Pushin, A. I. Lotkov, Yu. R. Kolobov, R. Z. Valiev, E. F. Dudarev, N. N. Kuranova, A. P. Dyupin, D. V. Gunderov, and G. P. Bakach, Phys. Met. Metallogr. **106**, 520 (2008).
8. U. Sari and T. Kirindi, Mater. Charact. **59**, 920 (2008).
9. A. Creuziger and W. C. Crone, Mater. Sci. Eng., A **498**, 404 (2008).
10. Z. Wang, X. F. Liu, and J. X. Xie, Prog. Natur. Sci.: Mater. Int. **21**, 368 (2011).
11. Z. Wang, X. F. Liu, and J. X. Xie, Mater. Sci. Eng., A **532**, 536 (2012).
12. G. Lojen, M. Cojic, and I. Anzel, J. Alloy Compd. **580**, 497 (2013).
13. P. Sedlak, H. Seiner, M. Landa, V. Novák, P. Šittner, and L. I. Manosa, Acta Mater. **53**, 3643 (2005).
14. V. N. Khachin, S. A. Muslov, V. G. Pushin, and Yu. I. Chumlyakov, Sov. Phys. Dokl. **32**, 606 (1987).
15. P. Rodriguez and G. Guenin, Mater. Sci. Eng., A **129**, 273 (1990).
16. H. Fu, S. Song, L. Zhuo, Z. Zhang, and J. Xie, Mater. Sci. Eng., A **650**, 218 (2016).
17. A. V. Lukyanov, V. G. Pushin, N. N. Kuranova, A. E. Svirid, A. N. Uksusnikov, Yu. M. Ustyugov, and D. V. Gunderov, Phys. Met. Metallogr. **119**, 374 (2018).
18. A. E. Svirid, N. N. Kuranova, A. V. Luk'yanov, V. V. Makarov, N. V. Nikolaeva, V. G. Pushin, and A. N. Uksusnikov, Russ. Phys. J. **61**, 1681 (2018).
19. V. G. Pushin, V. V. Stolyarov, R. Z. Valiev, N. I. Kourov, N. N. Kuranova, E. A. Prokofiev, and L. I. Yurchenko, Ann. Chim. Sci. Mater. **27**, 77 (2002).
20. V. G. Pushin, V. V. Stolyarov, R. Z. Valiev, T. C. Lowe, and Y. T. Zhu, Mater. Sci. Eng., A **410**, 386 (2005).

Translated by A. Bannov